Communication

Imprinted Apportionment of Functional Groups in Multivariate Metal-Organic Frameworks

Liang Feng, Kun-Yu Wang, Xiu-Liang Lv, Joshua A. Powell, Tianhao Yan, Jeremy Willman, and Hong-Cai Zhou

J. Am. Chem. Soc., **Just Accepted Manuscript** • Publication Date (Web): 04 Sep 2019

Imprinted Apportionment of Functional Groups in Multivariate Metal-Organic Frameworks

Liang Feng[†], Kun-Yu Wang[†], Xiu-Liang Lv[†], Joshua A. Powell[†], Tian-Hao Yan[†], Jeremy Willman[†], and Hong-Cai Zhou*[†§]

[†] Department of Chemistry, Texas A&M University, College Station, Texas 77843-3255, United States

[§] Department of Materials Science and Engineering, Texas A&M University, College Station, Texas 77843-3003, United States

Supporting Information Placeholder

ABSTRACT: Sophisticated chemical processes widely observed in biological cells require precise apportionment regulation of building units, which inspires researchers to develop tailorable architectures with controllable heterogeneity for replication, recognition and information storage. However, it remains a substantial challenge to endow multivariate materials with internal sequences and controllable apportionments. Herein, we introduce a novel strategy to manipulate the apportionment of functional groups in multivariate metal-organic frameworks (MTV-MOFs) by pre-incorporating interlocked linkers into framework materials. As a proof of concept, the imprinted apportionment of functional groups within ZIF-8 was achieved by exchanging imine-based linker templates with original linkers initially. The removal of linker fragments by hydrolysis can be achieved via post-synthetic labilization, leading to the formation of architectures with controlled heterogeneity. The distributions of functional groups in the resulting imprinted MOFs can be tuned by judicious control of the interlocked chain length, which was further analyzed by computational methods. This work provides synthetic tools for precise control of pore environment and functionality sequences inside multi-component materials.

The well-defined sequences and apportionment of multiple building units in biomolecules have inspired researchers to develop tailored architectures with controllable heterogeneity in polymers, nanomaterials and porous materials.[1-5] For example, multi-component metal–organic frameworks (MOFs) have recently gained increasing attention due to their enhanced sorption and separation behaviors, efficient cooperative catalytic activities and programmable luminescence or guest delivery behaviors.[6-15] For multi-component MOFs with linkers taking different crystallographic positions, functional groups can be precisely placed into predetermined positions (**Scheme S1a**).[16-19] Although the positions and arrangements of functional groups are fixed and ordered in this case, placement of linkers in fixed positions presents a lack of tunability over linker distances, interactions, apportionments and thus overall properties. Another set of mixed-linker MOFs, known as multivariate (MTV) MOFs, contains multiple types of linkers at identical crystallographic positions. MTV-MOF-5 and MTV-UiO-66 are representative MTV-MOFs synthesized using a one-pot approach (**Scheme S1b**).[20-21] In this case, the apportionment of the newly introduced functionalities is usually determined by characterization after synthesis, while *ab initio* construction of MTV-MOFs with predictable arrangement is almost impossible to achieve during the "black-box" synthesis.[11] In addition, post-synthetic linker exchange can alter the apportionment modes depending on the diffusion and exchange kinetics.[22-23] However, the mechanism of linker exchange and the influence of ligand sterics on the apportionment are far from fully understood. Therefore, novel strategies to regulate apportionment of functional groups in MTV-MOFs are an urgent need and will create new and unexpected opportunities for data recognition, replication, storage and delivery.

One possible solution is to synthesize MTV-MOFs *ab initio* with enhanced interactions between various functional groups.[24-26] For instance, cleavable covalent links between the functional groups on linkers can be judiciously introduced during a pre-synthetic step, and maintain this pre-interlocked sequence during the incorporation step. Subsequent cleavage of interlocking groups in the resultant heterogeneity-controlled imprinted MTV-MOFs will produce an MTV-MOF with precisely apportioned functional groups (**Scheme S1c**). Herein, we introduce a novel strategy to regulate apportionment of functional groups in MTV-MOFs by forming a pre-interlocked template. Initially, a pre-interlocked linker with cleavable links is incorporated inside the MTV-MOF under mild post-synthetic conditions. The control of apportionment and sequence is directed and ensured by the fixed covalent links within frameworks. These labile linkages between functionalized linkers are then selectively cleaved in the framework through hydrolysis, leading to the exposure of functional groups at correlated positions. Eventually, controlled heterogeneity in MTV-MOFs can be easily achieved by regulating apportionment of functionalities.

One of the most studied MOFs, ZIF-8, was introduced as a model to demonstrate our strategy because of its excellent stability and strong tolerance towards post-synthetic modification.[27-29] An aldehyde-based linker, denoted as Im-CHO (2-imidazolecarboxaldehyde), was chosen as a prototype to study the controlled heterogeneity within the framework while 2-methylimidazole (2-MeIm) is main matrix for dispersion. In order to form a pre-locked linker template (LX, X = 2, 3, 4, 6, 8 and 12, **Figure 1a**), Im-CHO was firstly linked to diamines

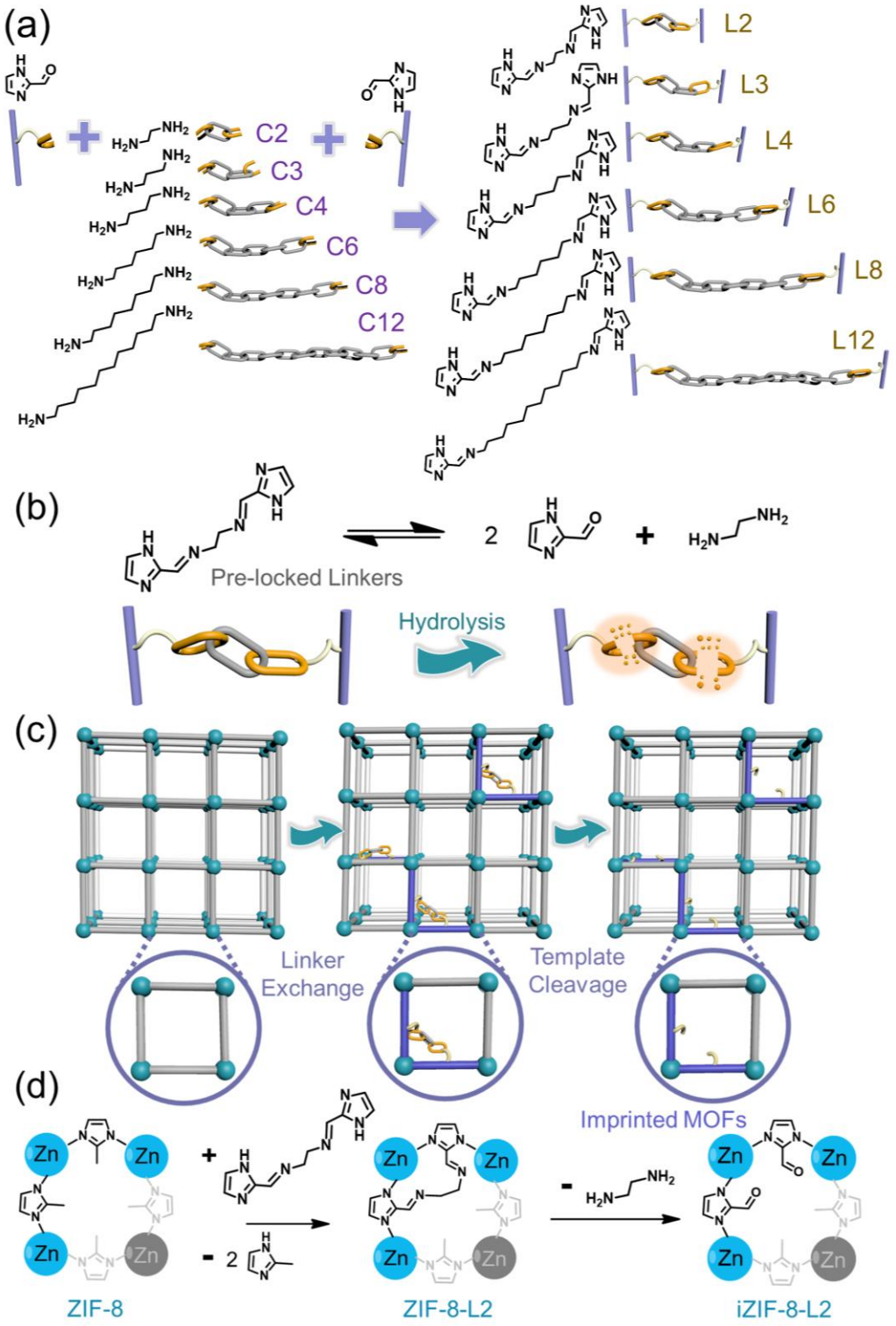

Figure 1. Controlled heterogeneity in MTV-MOFs: (a) The synthesis of pre-locked linkers (LX, X = 2, 3, 4, 6, 8 and 12). (b) The dissociation and association of imine bonds in pre-locked linker (L2); (c, d) Illustration of the sequential linker exchange and dissociation processes.

(CX, X = 2, 3, 4, 6, 8 and 12), to form a pre-labile linker, which can easily dissociate into the corresponding monomers in a single step through hydrolysis (**Figure 1b**).[30-31] Post-synthetic linker exchange at a mild condition (LX/MeOH solutions at 60 °C) was adopted (**Figure 2**), which shall maintain the integrity of the imine bonds in pre-locked linker templates (LX).[32] Relatively low concentration solutions of LX (15-30 mM) were utilized to minimize the possibility of a "dangling" exchange mode (**Figure S18**). After exchange, the crystals underwent a color change from white to light yellow as indicated by the optical images (**Figure 2a-d**). The preservation of the imine bonds after soaking in MeOH at 60°C for 24 h was verified by ^{1}H NMR spectroscopy (**Figure S13**). ^{1}H NMR spectroscopy of digested samples also demonstrated that both

imidazoles of LX successfully replaced the original 2-MeIm linkers (**Figure S18**), verifying that the exchange of LX happens in a locking/bridging mode. The exchanged ZIF-8 was denoted as ZIF-8-LX-R%, where the exchange ratio (R%) was defined as moles of imidazole from pre-locked linkers (LX) divided by the moles of total imidazole in exchanged ZIF-8. It was found that the exchange ratio R% of ZIF-8-L6-R% gradually increased as incubation time increased and leveled off after 300 min (**Figure 2e**). Further elongation of incubation time did not increase the L6 content, indicating that a dynamic equilibrium is reached between the solid and the solution. The exchange ratios of ZIF-8-L6 vary from 18% to 26%, when incubated with different concentrations of L6/MeOH solutions (15 and 30 mM, respectively) for 10 h. The supernatants after linker exchange were analyzed by ICP-MS, which showed no detectable Zn^{2+}. ZIF-8-LX-R% samples also maintain crystallinity as revealed by the PXRD patterns (**Figure S1-2**) and the microscope images of the respective crystals (**Figure 2b-d**). The N_2 adsorption isotherms of ZIF-8-L6-R% after post-synthetic linker exchange showed a clear decrease of N_2 total uptake compared with as-synthesized ZIF-8, corresponding to the cavity being filled by the newly-introduced bulky linkers with removable diamine linkages (**Figure 2f and Figure S6**). Additionally, the BET surface areas of ZIF-8 decreased after exchange because of the partially occupied pore spaces (**Table S3**).

The successful incorporation of pre-locked linkers in MTV-ZIF-8 can also be confirmed by comparing the diffuse reflectance infrared Fourier transform spectroscopy (DRIFTS) of ZIF-8 and ZIF-8-LX-R%. The appearance of imine bonds in ZIF-8-LX-R% is confirmed by the associated peaks [ν(C=N) at ~1651 cm^{-1}]. The composition of exchanged ZIF-8 was further

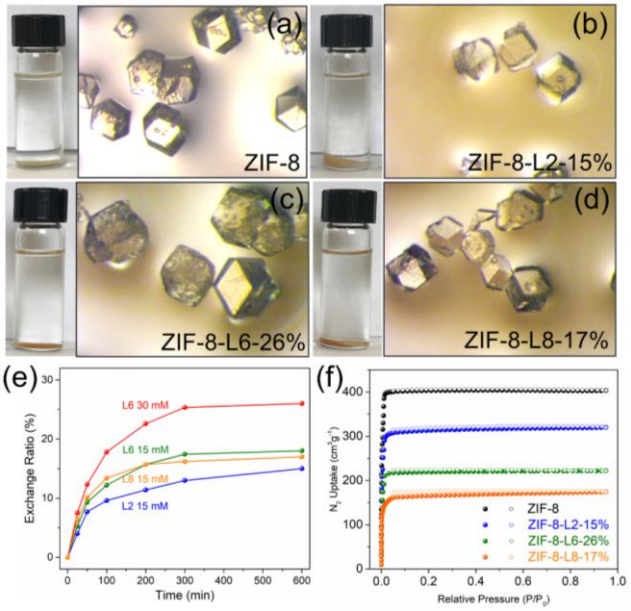

Figure 2. Monitoring linker exchange in ZIF-8: (a-d) Optical images of ZIF-8 before and after exchange; (e) Relationship between exchange ratio, period and linker (LX) concentration during exchange process; (f) N_2 sorption isotherms of ZIF-8-LX-R%.

analyzed by TGA (**Figures S22-23, Table S4-5**). The initial weight loss before 200 °C is attributed to the removal of the solvent molecules in the pores whereas the removal of organic

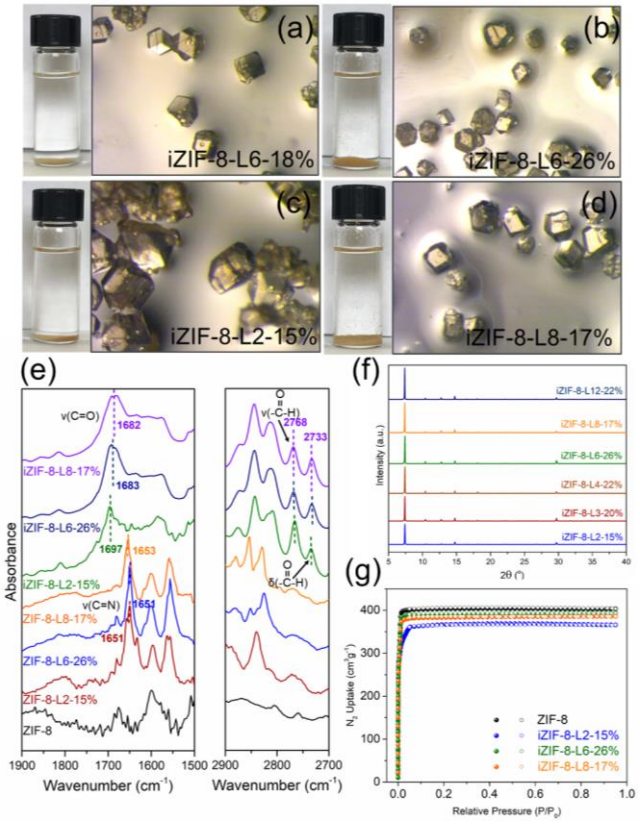

Figure 3. Studying linker dissociation in iZIF-8: (a-d) Optical images, (e) DRIFTS spectra, (f) PXRD patterns and (g) N_2 sorption isotherms of imprinted ZIF-8 crystals after linker dissociation.

linkers corresponds to the weight loss from 200 to 500 °C (**Figure S16**). Notably, ZIF-8-L6-26% shows much higher weight loss than ZIF-8 without post-synthetic treatment between 200 to 500 °C, due to the removal of the pre-locked linkages inside frameworks. These results show that the exchange ratio of ZIF-8 can be tuned with retention of framework integrity and porosity, which ensures the imprinted apportionment of functional groups in MTV-MOFs. Solid-state NMR spectroscopy of exchanged ZIFs indicates the complete deprotonation of templated linkers, which rules out the dangling possibility during the exchange process (**Figure S19-21**).

When exposed to aqueous solution, the pre-locked linkers (LX) in the framework were expected to dissociate into 2-methylimidazole and diamines (CX) through hydrolysis. When performed at room temperature for 24 h, the reaction between L6 and water does not go to completion (**Figure S11**). However, when the hydrolysis is performed at 50 °C, nearly quantitative cleavage of the imine bonds was observed, generating exposed aldehyde functional groups and released diamines (**Figure S12**). The cleaved diamines can be easily removed from the framework with sufficient washing, while the exposed functional groups (-CHO) are apportioned in a controlled fashion and manipulated by the tunable pre-locked chains. The resulting imprinted MTV-MOFs were donated as iZIF-8-LX-R%, where i stands for "imprinted". Note that the coordination bonds between Zn nodes and imidazole linkers are robust enough to survive from the mild water treatment.[33]

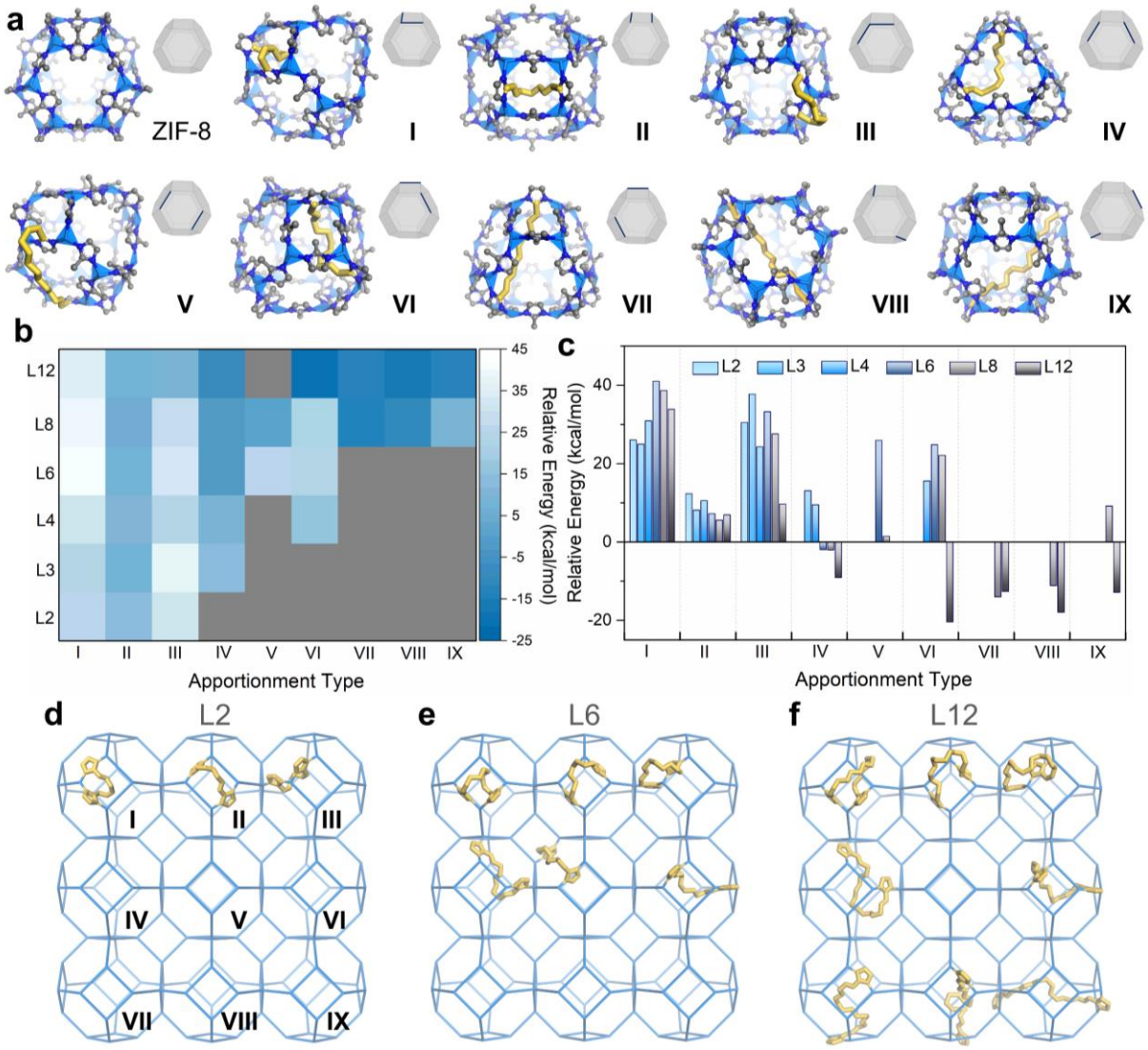

Figure 4. (a) The cage structure of ZIF-8 and nine possible apportionment types with linked template linkers LX; (b-c) Illustration of energy changes (unit: kcal/mol) after the exchange of 2-methylimidazole pairs with a chain template (LX, X = 2, 3, 4, 6, 8 and 12); (d-f) Illustration of possible link modes of L2, L6 and L12 within ZIF-8 cages.

ZIF-8 samples with various exchange ratios were prepared and treated with aqueous solution at 50 °C for 24 h. PXRD patterns of the resulting iZIF-8-LX-R% showed that the MOF materials after hydrolysis possessed the same diffraction patterns as the parent ZIF-8 (**Figure 3f**). The microscope images of the respective crystals demonstrated that the crystal morphology was not affected by the template cleavage process (**Figure 3a-d**). The porosity of iZIF-8-LX-R% was also studied by N_2 sorption measurements, which confirm an increase in pore size due to the release of template molecules. Compared to ZIF-8-LX-R%, the N_2 sorption isotherms of microporous iZIF-8-LX-R% at 77 K demonstrated increased uptakes with a type-I isotherm, indicating the release of template molecules from the framework (**Figure 3g**). No notable mesopores were observed in the N_2 sorption isotherms, ruling out the possibility of partial decomposition of ZIF-8 during post-synthetic treatment. The subsequent cleavage of pre-locked linkers significantly changed the pore volume and corresponding environment.

To examine whether the imine bonds were successfully dissociated during the hydrolysis treatment, DRIFTS absorption spectroscopy was utilized to confirm the linker dissociation process. As evidenced by **Figure 3e**, a clear blue shift of the stretching bands of the imine group [ν(C=N), ~1651 cm^{-1}] to aldehyde group [ν(C=O), ~1683 cm^{-1}] was observed. Besides, there are also appearance of peaks around 2768 cm^{-1} and 2733 cm^{-1}, associated with ν(C-H, aldehyde) and δ(C-H, aldehyde) modes, respectively, which indicates successful cleavage of the imine bond. In addition, the composition of iZIF-8 was further analyzed by TGA and compared with ^{1}H NMR results (**Figures S14-16**). The weight losses corresponding to the thermal decomposition of organic fragments match well with the calculation.

We further extended the strategy to other diamines with various chain lengths to investigate the versatility of regulated apportionment of pre-locked linkers. Six pre-locked linkers were introduced with variable lengths to regulate the distribution of functional groups in the ordered frameworks. The successful sequential linker exchange and dissociation were achieved in these systems with well-maintained crystallinity, as indicated by optical images, N_2 sorption isotherms, and

PXRD patterns (**Figure S2**). To gain insights into the controlled linker apportionment in iZIF-8-LX-R%, we inspected the possible models of linker apportionment to study the distances and distributions of ZIF frameworks. We found that spatial distributions of pre-locked linker templates (LX) could be influenced by the distance and orientation of imidazole ligands in original frameworks. The ZIF cage was modelled as a truncated octahedron, with the zinc nodes represented by the vertices and the ligands represented by the edges of the polyhedron (**Figure 4a**). Faces of the polyhedron are comprised of squares and hexagons. For conciseness, the spatial relationship between ligands can be displayed through a projection on the polyhedron. The orientations of two imidazole ligands can be described as one of four different patterns: opposite, inverse, parallel, and anti-parallel. According to the calculation results, the opposite and parallel patterns are the most favored, while the inverse pattern is almost impossible because of the torsional strain it imposes on LX. Therefore, a total of nine possible apportionment patterns, labeled from I to IX, can be found within a ZIF cage (**Figure 4a**).

According to density-functional calculations performed by the DMol³ program of Materials Studio, relative energies of substitution can be obtained by subtracting the energy of ZIF-8 and LX from that of ZIF-8-LX (**Figure 4b-c**).[34] Remarkably, for LX with a longer chain length, more diverse substitution patterns can be accessed (**Figure S24**). In general, the results shown that a shorter linker tends to connect adjacent positions with parallel ligands because of the length limitation, while for a longer linker, although with increased freedom and length, its torsion strain becomes a dominant factor for spatial distribution, as a result, it prefers a non-distortion pattern and substitutes two distant opposite ligands (**Figure 4, Table S6**). Our results here exemplify the idea of *ab initio* synthesis with predictable arrangement of functional groups within MTV-MOFs, which provides a tool for sequence manipulation in multi-component materials.

ASSOCIATED CONTENT

Supporting Information. This material is available free of charge on the ACS Publications website at DOI: xxxxxxxxxx.

Synthetic procedures for organic ligands and MOF materials, analysis of linker exchange and dissociation including PXRD patterns, SEM data, NMR analysis and TGA analysis (PDF)

AUTHOR INFORMATION

Corresponding Author

*zhou@chem.tamu.edu

Notes

The authors declare no competing financial interests.

ACKNOWLEDGMENT

The gas adsorption-desorption studies of this research were supported by the Center for Gas Separations, an Energy Frontier Research Center funded by the U.S. Department of Energy, Office of Science, Office of Basic Energy Sciences under Award Number DE-SC0001015. The synthesis and structural characterization were supported by the Robert A. Welch Foundation through a Welch Endowed Chair to H.-C. Z (A-0030). We acknowledge the experimental assistance and insightful discussion with Dr. Vladimir Bakhmoutov and Mr. Jialuo Li.

REFERENCES

1. Lutz, J. F.; Ouchi, M.; Liu, D. R.; Sawamoto, M., Sequence-Controlled Polymers. *Science* **2013,** *341* (6146), 628.
2. Bates, F. S.; Hillmyer, M. A.; Lodge, T. P.; Bates, C. M.; Delaney, K. T.; Fredrickson, G. H., Multiblock Polymers: Panacea or Pandora's Box? *Science* **2012,** *336* (6080), 434-440.
3. Marcos, V.; Stephens, A. J.; Jaramillo-Garcia, J.; Nussbaumer, A. L.; Woltering, S. L.; Valero, A.; Lemonnier, J. F.; Vitorica-Yrezabal, I. J.; Leigh, D. A., Allosteric initiation and regulation of catalysis with a molecular knot. *Science* **2016,** *352* (6293), 1555-1559.
4. Matyjaszewski, K., Architecturally Complex Polymers with Controlled Heterogeneity. *Science* **2011,** *333* (6046), 1104-1105.
5. Kametani, Y.; Sawamoto, M.; Ouchi, M., Control of the Alternating Sequence for N-Isopropylacrylamide (NIPAM) and Methacrylic Acid Units in a Copolymer by Cyclopolymerization and Transformation of the Cyclopendant Group. *Angew. Chem. Int. Ed.* **2018,** *57* (34), 10905-10909.
6. Popp, T. M. O.; Yaghi, O. M., Sequence-Dependent Materials. *Acc. Chem. Res.* **2017,** *50* (3), 532-534.
7. Zhou, H. C.; Long, J. R.; Yaghi, O. M., Introduction to Metal-Organic Frameworks. *Chem. Rev.* **2012,** *112* (2), 673-674.
8. Kirchon, A.; Feng, L.; Drake, H. F.; Joseph, E. A.; Zhou, H. C., From fundamentals to applications: a toolbox for robust and multifunctional MOF materials. *Chem. Soc. Rev.* **2018**, 47, 8611-8638.
9. Zhou, H. C.; Kitagawa, S., Metal-Organic Frameworks (MOFs). *Chem. Soc. Rev.* **2014,** *43* (16), 5415-5418.
10. Helal, A.; Yamani, Z. H.; Cordova, K. E.; Yaghi, O. M., Multivariate metal-organic frameworks. *Natl. Sci. Rev.* **2017,** *4* (3), 296-298.
11. Kong, X. Q.; Deng, H. X.; Yan, F. Y.; Kim, J.; Swisher, J. A.; Smit, B.; Yaghi, O. M.; Reimer, J. A., Mapping of Functional Groups in Metal-Organic Frameworks. *Science* **2013,** *341* (6148), 882-885.
12. Feng, L.; Yuan, S.; Li, J. L.; Wang, K. Y.; Day, G. S.; Zhang, P.; Wang, Y.; Zhou, H. C., Uncovering Two Principles of Multivariate Hierarchical Metal-Organic Framework Synthesis via Retrosynthetic Design. *ACS Cent. Sci.* **2018,** *4* (12), 1719-1726.
13. Feng, L.; Li, J.-L.; Day, G. S.; Lv, X.-L.; Zhou, H.-C., Temperature-Controlled Evolution of Nanoporous MOF Crystallites into Hierarchically Porous Superstructures. *Chem* **2019,** 5, 1265-1274.
14. Cornelio, J.; Zhou, T.-Y.; Alkaş, A.; Telfer, S. G., Systematic Tuning of the Luminescence Output of Multicomponent Metal–Organic Frameworks. *J. Am. Chem. Soc.* **2018,** *140* (45), 15470-15476.
15. Zhou, T.-Y.; Auer, B.; Lee, S. J.; Telfer, S. G., Catalysts Confined in Programmed Framework Pores Enable New Transformations and Tune Reaction Efficiency and Selectivity. *J. Am. Chem. Soc.* **2019,** *141* (4), 1577-1582.
16. Yuan, S.; Chen, Y.-P.; Qin, J.-S.; Lu, W.; Zou, L.; Zhang, Q.; Wang, X.; Sun, X.; Zhou, H.-C., Linker installation: engineering pore environment with precisely placed functionalities in zirconium MOFs. *J. Am. Chem. Soc.* **2016,** *138* (28), 8912-8919.
17. Yuan, S.; Lu, W.; Chen, Y.-P.; Zhang, Q.; Liu, T.-F.; Feng, D.; Wang, X.; Qin, J.; Zhou, H.-C., Sequential linker installation: precise placement of functional groups in multivariate metal–organic frameworks. *J. Am. Chem. Soc.* **2015,** *137* (9), 3177-3180.
18. Liu, L.; Konstas, K.; Hill, M. R.; Telfer, S. G., Programmed pore architectures in modular quaternary metal–organic frameworks. *J. Am. Chem. Soc.* **2013,** *135* (47), 17731-17734.

19. Liu, L.; Telfer, S. G., Systematic ligand modulation enhances the moisture stability and gas sorption characteristics of quaternary metal–organic frameworks. *J. Am. Chem. Soc.* **2015,** *137* (11), 3901-3909.
20. Deng, H. X.; Doonan, C. J.; Furukawa, H.; Ferreira, R. B.; Towne, J.; Knobler, C. B.; Wang, B.; Yaghi, O. M., Multiple Functional Groups of Varying Ratios in Metal-Organic Frameworks. *Science* **2010,** *327* (5967), 846-850.
21. Feng, L.; Yuan, S.; Zhang, L. L.; Tan, K.; Li, J. L.; Kirchon, A.; Liu, L. M.; Zhang, P.; Han, Y.; Chabal, Y. J.; Zhou, H. C., Creating Hierarchical Pores by Controlled Linker Thermolysis in Multivariate Metal-Organic Frameworks. *J. Am. Chem. Soc.* **2018,** *140* (6), 2363-2372.
22. Boissonnault, J. A.; Wong-Foy, A. G.; Matzger, A. J., Core-Shell Structures Arise Naturally During Ligand Exchange in Metal-Organic Frameworks. *J. Am. Chem. Soc.* **2017,** *139* (42), 14841-14844.
23. Fluch, U.; Paneta, V.; Primetzhofer, D.; Ott, S., Uniform distribution of post-synthetic linker exchange in metal-organic frameworks revealed by Rutherford backscattering spectrometry. *Chem. Commun.* **2017,** *53* (48), 6516-6519.
24. Gallego, E. M.; Portilla, M. T.; Paris, C.; Leon-Escamilla, A.; Boronat, M.; Moliner, M.; Corma, A., "Ab initio" synthesis of zeolites for preestablished catalytic reactions. *Science* **2017,** *355* (6329).
25. Allen, C. A.; Boissonnault, J. A.; Cirera, J.; Gulland, R.; Paesani, F.; Cohen, S. M., Chemically crosslinked isoreticular metal-organic frameworks. *Chem. Commun.* **2013,** *49* (31), 3200-3202.
26. Allen, C. A.; Cohen, S. M., Exploration of Chemically Cross-Linked Metal-Organic Frameworks. *Inorg. Chem.* **2014,** *53* (13), 7014-7019.
27. Liu, C. Y.; Liu, Q.; Huang, A. S., A superhydrophobic zeolitic imidazolate framework (ZIF-90) with high steam stability for efficient recovery of bioalcohols. *Chem. Commun.* **2016,** *52* (16), 3400-3402.
28. Jayachandrababu, K. C.; Sholl, D. S.; Nair, S., Structural and Mechanistic Differences in Mixed-Linker Zeolitic Imidazolate Framework Synthesis by Solvent Assisted Linker Exchange and de Novo Routes. *J. Am. Chem. Soc.* **2017,** *139* (16), 5906-5915.
29. Park, K. S.; Ni, Z.; Cote, A. P.; Choi, J. Y.; Huang, R. D.; Uribe-Romo, F. J.; Chae, H. K.; O'Keeffe, M.; Yaghi, O. M., Exceptional chemical and thermal stability of zeolitic imidazolate frameworks. *Proc. Natl. Acad. Sci. USA* **2006,** *103* (27), 10186-10191.
30. Yuan, S. A.; Zou, L. F.; Qin, J. S.; Li, J. L.; Huang, L.; Feng, L. A.; Wang, X. A.; Bosch, M.; Alsalme, A.; Cagin, T.; Zhou, H. C., Construction of hierarchically porous metal-organic frameworks through linker labilization. *Nat. Commun.* **2017,** *8,* 15356.
31. Feng, L.; Yuan, S.; Qin, J.-S.; Wang, Y.; Kirchon, A.; Qiu, D.; Cheng, L.; Madrahimov, S. T.; Zhou, H.-C., Lattice Expansion and Contraction in Metal-Organic Frameworks by Sequential Linker Reinstallation. *Matter* **2019,** 1 (1), 156-167.
32. Cohen, S. M., Postsynthetic methods for the functionalization of metal-organic frameworks. *Chem Rev* **2012,** *112* (2), 970-1000.
33. Yuan, S.; Feng, L.; Wang, K.; Pang, J.; Bosch, M.; Lollar, C.; Sun, Y.; Qin, J.; Yang, X.; Zhang, P.; Wang, Q.; Zou, L.; Zhang, Y.; Zhang, L.; Fang, Y.; Li, J.; Zhou, H. C., Stable Metal–Organic Frameworks: Design, Synthesis, and Applications. *Adv. Mater.* **2018**, 1704303.
34. Delley, B., From molecules to solids with the DMol 3 approach. *J. Chem. Phys.* **2000,** *113* (18), 7756-7764.

Table of Contents